

Modelisation and simulation of the light collection in the CMS lead tungstate crystals

R. Chipaux, M. Géléoc

CEA DAPNIA/SED, Saclay, France

Abstract

The ageing of scintillating crystals under radiation leads to a deterioration of their transparency, thus of their effective light yield and their calibration. The link between the transparency variation, as measured by a fibre optic monitoring system, and the calibration variation is not trivial. A model describing the light collection process is proposed. It helps to understand the parameters which govern this correlation, mainly absorption length and light back-reflection or diffusion characteristics. This model describes well the results of numerical qualitative simulations of light collection in lead tungstate crystals. It also explains the differences between calibration and monitoring variations observed in test beam.

Keywords : Scintillator detector, light yield, ray tracing simulation, ageing, radiation damage.

PACS : 29.40.Mc ; 78.20.Bh ; 61.80.Az.

submitted to *Nuclear Instruments and Methods in Physics Research A*

1 Introduction

In scintillating crystal detectors exposed to high flux of radiation, like the lead tungstate electromagnetic calorimeter of the future CMS experiment at the Large Hadron Collider in construction at CERN [1, 2], a monitoring of calibration coefficients throughout the life of the experiment is mandatory [3, 4]. Continuous calibration with physical events of known energy is highly desirable. However it is not always possible to obtain sufficient statistics in short time to cope with fast variations, for example when the crystals present a degradation or a recovery of their optical transparency, even limited in amplitude, at low dose or fluence, as reported in [5].

It is consequently necessary to monitor continuously the optical properties of the crystals, by injecting calibrated light pulses and measuring them in the same manner as the physical events. However injected and scintillation lights do not have the same characteristics : wavelength spectra, angular apertures and optical paths are not identical. Thus it is not expected that the two signals vary proportionally. Their variations are nevertheless highly correlated and this correlation depends on the optical characteristics, in general sense, of crystals and photodetectors, and may vary from crystal to crystal. The parameters governing this correlation should be understood, and the correlation quantified, to perform a precise correction of the calibration constants knowing the variation of the monitoring signal.

Being in charge of the realisation of the light monitoring system, we have approached in Saclay this crucial problem from several points of view : theoretical, experimental, numerical, etc. [4, 6, 7]. One presents here a tentative modelisation of the light collection in scintillating crystals for monitoring and scintillation lights, confronted with the results of a ray tracing Monte-Carlo program.

2 Modelisation

The monitoring system sends light pulses to the front of the crystals, the photodetector being at the rear, and to reference photodiodes. For a given crystal, the corresponding signal could be expressed as :

$$S_m(t, \lambda) = a(t, \lambda)L(t, \lambda)C_m(t, \lambda)\bar{M}(t, \lambda) \quad (1)$$

where a describes the relative light transmission of the fibre, L is the number of photons arriving at the same time on the reference photodiode, C_m is the effective transmission of the crystal for the injected light, \bar{M} the product of the quantum efficiency of the photodetector by its gain.

In the same way, the scintillation signal due to particles could be parametrized, for a given crystal, in :

$$S_s(t, E_0) = E_0 \int_{\lambda} \int_0^L N(E_0, z)C_s(t, z, \lambda)P(t, z, \lambda)\bar{M}(t, \lambda)d\lambda dz \quad (2)$$

where E_0 is the energy deposited by the particle in the crystal, N the density of this energy deposition along z , which depends on type, energy and direction of the incident particle, P the scintillation spectrum (in photon per unit of energy), and C_s the effective transmission of the crystal for the scintillation light. For simplicity, dependencies on temperature and electrical polarization have not been indicated explicitly in the above expressions, notably for \bar{M} and P . See reference [3, 4] for more details.

As shown in [8, 9], radiation does not affect the scintillation mechanism in the crystals for the dose and fluence ranges considered in CMS. In the time scale considered by the monitoring system, the main factor of variation is, as above mentioned, the variation of transparency of the crystals due to radiation. The discussion will be restrained hereafter to the transmission terms C_m and C_s , assuming that other parameters are constant, or that they vary with longer time scales. In particular the effect of temperature variation on scintillation and apd response will be neglected, as well as the long term ageing. In a first step, one also assumes for simplicity that attenuation of light in crystals is homogeneous, and can be described by an absorption length Λ :

$$\frac{1}{\Lambda(t, \lambda)} = \frac{1}{\Lambda(0, \lambda)} + \mu(t, \lambda) = \frac{1}{\Lambda_0(\lambda)} + \mu(t, \lambda) \quad (3)$$

where μ is the induced absorption coefficient.

2.1 Monitoring

One considers here the scheme held for the CMS barrel electromagnetic calorimeter, that is light injection by optical fibres on the face opposite to the photodetector. One quantifies first the “direct” transmission, that is the proportion of light which reach directly the photodetector, travelling through the length of the crystal. Then, introducing reflections on front and rear faces, one quantifies the “multiple turn” transmission, that is the proportion of light that encounter successive reflection on the front and back faces before being detected. The total transmission is obviously the sum these two quantities. The argumentation would be very similar for other geometries, like injection from the photodetector side as foreseen in the end cap calorimeter.

The direct transmission can be approximated by :

$$\begin{aligned} C_{m_d}(t, \lambda) &= {}^x t_{m_d} {}^o t_{m_d} \exp\left(-\frac{b_{m_d} L}{\Lambda(t, \lambda)}\right) \\ &= C_{m_D} \exp\left(-\frac{b_{m_d} L}{\Lambda(t, \lambda)}\right) \end{aligned} \quad (4)$$

where

- ${}^x t_{m_d}$ is the proportion of light that would reach the output face in absence of internal absorption (that is if $\Lambda \rightarrow \infty$). It represents the loss of light due to surface imperfection, diffusion or any other source of light loss. (In absence of diffusion and for perfectly polished surfaces, the monitoring light will be always in total reflection on the lateral faces, and ${}^x t_{m_d} = 1$.)
- ${}^o t_{m_d}$ is the probability to be transmitted to the photodetector for a photon that has reached the output face. It take into account surface coverage and surface reflection, but not the quantum efficiency (included in \bar{M}).
- $b_{m_d} L$ is the mean length covered by the light, L being the crystal length. The monitoring light is characterized by a small angular aperture, due to the intrinsically small optical fibre aperture, which is furthermore reduced by the high index of refraction of the crystal. Thus, in absence of diffusion, one expects b_{m_d} to be very close to one.

To obtain the evolution from a starting point with finite absorption, one introduces the induced absorption coefficient. Defining $C_{m_{d_0}}(\lambda) = C_{m_d}(t = 0, \lambda)$, equation 4 becomes :

$$C_{m_d}(t, \lambda) = C_{m_{d_0}}(\lambda) \exp(-b_{m_d} L \mu(t, \lambda)) \quad (5)$$

One can introduce as a comparative parameter the sensitivity to transmission variation, given by the relative derivative of the transmission $C_m(t, \lambda)$ versus the induced absorption coefficient μ , in that case equal to the mean path :

$$R_{m_d}(t, \lambda) = \frac{-dC_{m_d}(t, \lambda)}{C_{m_d}(t, \lambda) d\mu(t, \lambda)} = b_{m_d} L \quad (6)$$

This parameter could be measured in laboratory, where $\mu(t, \lambda)$ could be determined, but obviously not in the final experiment.

Now, if one takes into account the reflections at the extremities, introducing the effective generalised reflection, transmission and length parameters ${}^i r_{m_i}$, ${}^o r_{m_i}$, ${}^o t_{m_i}$, ${}^x t_{m_i}$, b_{m_i} , equation 4 is changed in :

$$C_m(t, \lambda) = {}^x t_{m_d} \exp\left(-\frac{b_{m_d} L}{\Lambda(t, \lambda)}\right) \left({}^o t_{m_d} + {}^o r_{m_1} {}^i r_{m_1} {}^x t_{m_1}^2 \exp\left(-\frac{2b_{m_1} L}{\Lambda(t, \lambda)}\right) \left({}^o t_{m_1} + \right. \right. \\ \left. \left. {}^o r_{m_2} {}^i r_{m_2} {}^x t_{m_2}^2 \exp\left(-\frac{2b_{m_2} L}{\Lambda(t, \lambda)}\right) ({}^o t_{m_2} + \dots) \right) \right) \quad (7)$$

Assuming that successive reflections lead to identical parameters, that is that one can define :

$$\begin{aligned} {}^i r_m &= {}^i r_{m_1} = {}^i r_{m_2} = \dots \\ {}^o r_m &= {}^o r_{m_1} = {}^o r_{m_2} = \dots \\ {}^o t_m &= {}^o t_{m_1} = {}^o t_{m_2} = \dots \\ {}^x t_m &= {}^x t_{m_1} = {}^x t_{m_2} = \dots \\ b_m &= b_{m_1} = b_{m_2} = \dots \end{aligned} \quad (8)$$

one obtains :

$$\begin{aligned} C_m(t, \lambda) &= \frac{{}^x t_{m_d} {}^o t_{m_d} \exp\left(-\frac{b_{m_d} L}{\Lambda(t, \lambda)}\right)}{1 - {}^o r_m {}^i r_m {}^x t_m^2 \frac{{}^o t_m}{{}^o t_{m_d}} \exp\left(-\frac{2b_m L}{\Lambda(t, \lambda)}\right)} \\ &= \frac{C_{m_D} \exp\left(-\frac{b_{m_d} L}{\Lambda(t, \lambda)}\right)}{1 - k_m^2 \exp\left(-\frac{2b_m L}{\Lambda(t, \lambda)}\right)} \end{aligned} \quad (9)$$

if one defines the effective reflection coefficient k_m^2 by :

$$k_m^2 = {}^o r_m {}^i r_m {}^x t_m^2 \frac{{}^o t_m}{{}^o t_{m_d}} \quad (= {}^o r_m {}^i r_m {}^x t_m^2 \text{ if } {}^o t_m = {}^o t_{m_d}) \quad (10)$$

Introducing, as for equation 5, the initial transmission $C_{m_0}(\lambda) = C_m(t = 0, \lambda)$, one obtains :

$$\begin{aligned} C_m(t, \lambda) &= C_{m_0}(\lambda) \exp(-b_{m_d} L \mu(t, \lambda)) \frac{1 - k_m^2 \exp\left(-\frac{2b_m L}{\Lambda_0(\lambda)}\right)}{1 - k_m^2 \exp\left(-\frac{2b_m L}{\Lambda_0(\lambda)}\right) \exp(-2b_m L \mu(t, \lambda))} \\ &= C_{m_0}(\lambda) \frac{\sinh\left(\frac{b_m L}{\Lambda_0(\lambda)} - \log(k_m)\right)}{\sinh\left(\frac{b_m L}{\Lambda(t, \lambda)} - \log(k_m)\right)} \exp\left((b_m - b_{m_d}) L \mu(t, \lambda)\right) \end{aligned} \quad (11)$$

This equation is equivalent to equation 5 corrected by a factor due to the successive reflections and dependant on the initial absorption length Λ_0 and on the induced absorption coefficient μ .

The sensitivity to transmission degradation is given by :

$$\begin{aligned} R_m(t, \lambda) &= \frac{-dC_m(t, \lambda)}{C_m(t, \lambda)d\mu(t, \lambda)} = \left(b_{m_d} + \frac{2b_m}{\frac{1}{k_m^2} \exp\left(\frac{2b_m L}{\Lambda_o(\lambda)}\right) - 1} \right) L \\ &= \left(b_{m_d} + b_m \left(\coth\left(\frac{b_m L}{\Lambda_o(\lambda)}\right) - \log(k_m) + b_m L \mu(t, \lambda) \right) - 1 \right) L \end{aligned} \quad (12)$$

The successive reflections increase the mean path by a length equal to $b_m \left(\coth\left(\frac{b_m L}{\Lambda_o}\right) - \log(k_m) + b_m L \mu \right) - 1) L$. This accounts for the fact that not only the light yield, but even more the sensitivity to induced absorption increases when the effective reflection coefficient k_m^2 increases, notably when the initial transparency of the crystal is good. This effect is illustrated in figure 1.

In the calorimeter, the radiation dose received will be function of z and thus the induced absorption coefficient μ . It could be also the case for the initial absorption Λ_0 if the crystal is not homogeneous. The expression of $C_m(t, \lambda)$ remains similar, replacing $\exp\left(-\frac{bL}{\Lambda_0(\lambda)}\right)$ and $\exp(-bL\mu(t, \lambda))$ by the mean values $\exp\left(-\int_0^L \frac{bz}{\Lambda_0(\lambda, z)} dz\right)$ and $\exp\left(-\int_0^L bz\mu(t, \lambda, z) dz\right)$. Conclusions regarding the sensitivity to absorption are identical.

2.2 Scintillation

Unlike the monitoring light, the scintillation light is emitted isotropically, so that one half is emitted toward the photodetector and can reach it “directly”, and the other at the opposite and should be reflected at least once on the front face of the crystal before to be detected. Thus, for the scintillation light, the transmission should be decomposed in a “direct” part, an indirect or “back” part, and a “multiple turn” part

By analogy with the monitoring, the “direct” transmission, that is the proportion of scintillation light that reaches the photodetector without reflection on the front face, can be written as :

$$\begin{aligned} C_{s_d}(t, \lambda, z) &= {}^x t_{s_d} {}^o t_{s_d} \exp\left(-\frac{b_{s_d}(L-z)}{\Lambda(t, \lambda)}\right) \\ &= C_{s_D}(z) \exp\left(-\frac{b_{s_d}(L-z)}{\Lambda(t, \lambda)}\right) \end{aligned} \quad (13)$$

${}^x t_{s_d}$, ${}^o t_{s_d}$ and b_{s_d} have the same meaning for the scintillation light than ${}^x t_{m_d}$, ${}^o t_{m_d}$ and b_{m_d} for the monitoring light, but are function of z .

In the same way the “back” transmission, that is the proportion of light that reaches the photodetector after a reflection at the front face of the crystal, can be written as :

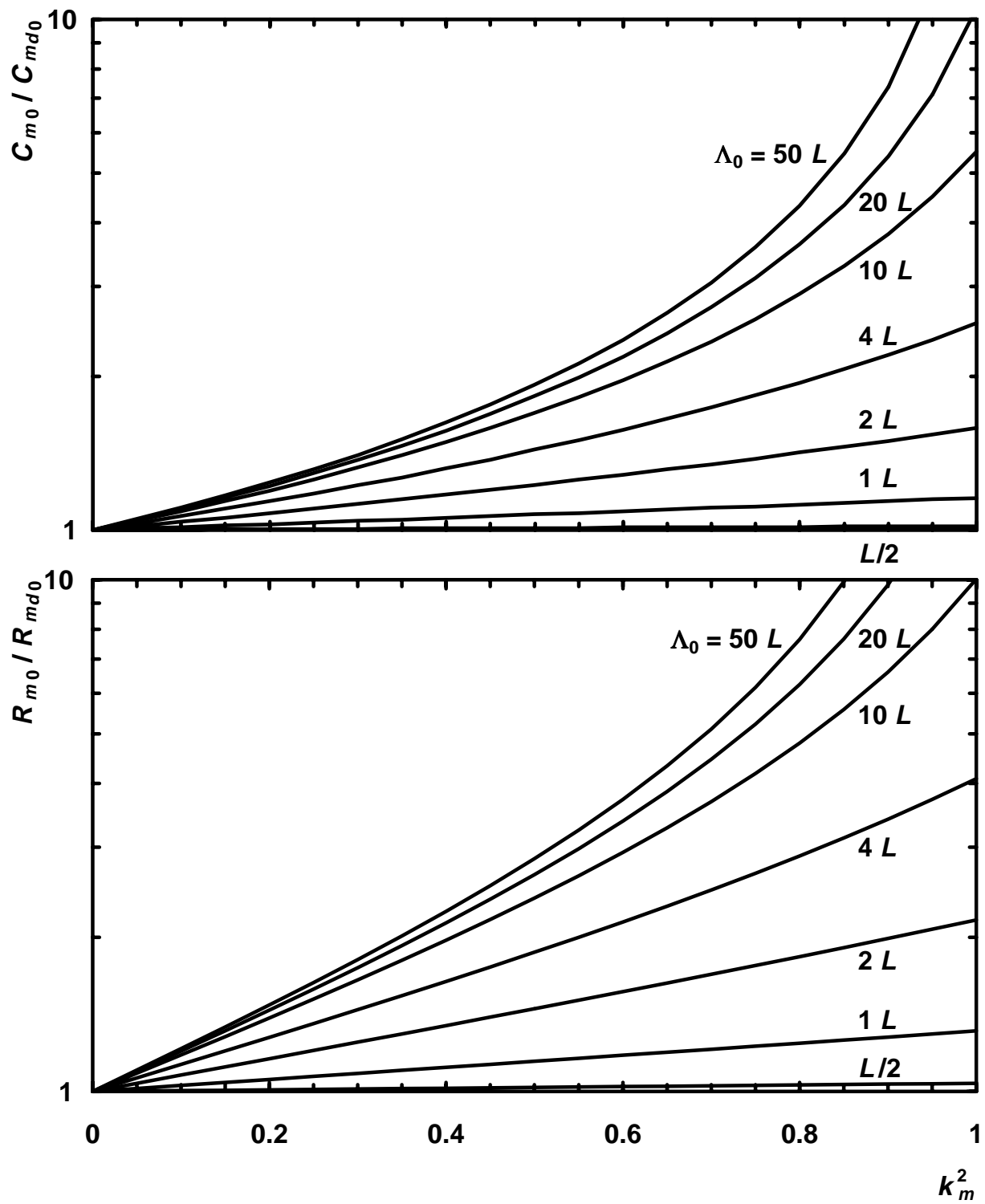


Figure 1: Monitoring light : variations of the initial effective transmission C_{m_0} , normalized to the transmission with absorbing ends (above), and of the initial sensitivity to absorption $R_{m_0} = R_m(t = 0)$, normalized to the sensitivity with absorbing ends (below), versus the effective reflection coefficient k_m^2 for various value of the initial absorption length Λ_0 , according to equations 9 and 12. L is the length of the crystal.

$$\begin{aligned}
C_{s_b}(t, \lambda, z) &= {}^x t_{s_b} {}^i r_{s_b} {}^o t_{s_b} \exp\left(-\frac{b_{s_b}(L+z)}{\Lambda(t, \lambda)}\right) \\
&= C_{s_B}(z) \exp\left(-\frac{b_{s_b}(L+z)}{\Lambda(t, \lambda)}\right)
\end{aligned} \tag{14}$$

Introducing the multiple reflections, one obtains :

$$\begin{aligned}
C_s(t, \lambda, z) &= C_{s_D}(z) \exp\left(-\frac{b_{s_d}(L-z)}{\Lambda(t, \lambda)}\right) \left(1 + {}^o r_{s_{d1}} {}^i r_{s_{d1}} {}^x t_{s_{d1}}^2 \exp\left(-\frac{2b_{s_{d1}}L}{\Lambda(t, \lambda)}\right) \left(\frac{{}^o t_{s_{d1}}}{{}^o t_{s_d}} + \right. \right. \\
&\quad \left. \left. {}^o r_{s_{d2}} {}^i r_{s_{d2}} {}^x t_{s_{d2}}^2 \exp\left(-\frac{2b_{s_{d2}}L}{\Lambda(t, \lambda)}\right) \left(\frac{{}^o t_{s_{d2}}}{{}^o t_{s_d}} + \dots\right)\right)\right) \\
&+ C_{s_B}(z) \exp\left(-\frac{b_{s_d}(L-z)}{\Lambda(t, \lambda)}\right) \left(1 + {}^o r_{s_{b1}} {}^i r_{s_{b1}} {}^x t_{s_{b1}}^2 \exp\left(-\frac{2b_{s_{b1}}L}{\Lambda(t, \lambda)}\right) \left(\frac{{}^o t_{s_{b1}}}{{}^o t_{s_d}} + \right. \right. \\
&\quad \left. \left. {}^o r_{s_{b2}} {}^i r_{s_{b2}} {}^x t_{s_{b2}}^2 \exp\left(-\frac{2b_{s_{b2}}L}{\Lambda(t, \lambda)}\right) \left(\frac{{}^o t_{s_{b2}}}{{}^o t_{s_d}} + \dots\right)\right)\right)
\end{aligned} \tag{15}$$

Again, assuming that successive reflections lead to identical parameters, one defines :

$$\begin{aligned}
{}^i r_s &= {}^i r_{s_{d1}} = {}^i r_{s_{b1}} = {}^i r_{s_{d2}} = \dots \\
{}^o r_s &= {}^o r_{s_{d1}} = {}^o r_{s_{b1}} = {}^o r_{s_{d2}} = \dots \\
{}^o t_s &= {}^o t_{s_{d1}} = {}^o t_{s_{b1}} = {}^o t_{s_{d2}} = \dots \\
{}^x t_s &= {}^x t_{s_{d1}} = {}^x t_{s_{b1}} = {}^x t_{s_{d2}} = \dots \\
b_s &= b_{s_{d1}} = b_{s_{b1}} = b_{s_{d2}} = \dots \\
{}^o t_s &= {}^o t_{s_d} = {}^o t_{s_b} \\
k_s^2 &= {}^o r_s {}^i r_s {}^x t_s^2
\end{aligned} \tag{16}$$

One obtains :

$$C_s(t, \lambda, z) = \frac{C_{s_D} \exp\left(-\frac{b_{s_d}(L-z)}{\Lambda(t, \lambda)}\right) + C_{s_B} \exp\left(-\frac{b_{s_b}(L+z)}{\Lambda(t, \lambda)}\right)}{1 - k_s^2 \exp\left(-\frac{2b_s L}{\Lambda(t, \lambda)}\right)} \tag{17}$$

3 Simulations

3.1 Description

The simulations presented here are based on the ray-tracing Monte-Carlo program *LUX* which has been developed for the qualitative simulation of light transmission in crystals [6]. In this program, crystals are considered as homogeneous and not diffusive in bulk nor in surface, various generic surfaces can be selected : fully absorbing, refractive, or covered with a perfectly reflective or diffusive wrapping.

This study uses : – for the crystals, tapered, $((20.5 \times 20.5) - (23.7 \times 23.7) \times 230 \text{ mm}^3)$ and parallelepipedic shapes, $(23.7 \times 23.7 \times 230 \text{ mm}^3)$, both without chamfers and with perfect surfaces, – for the photodetectors, an active surface of $5 \times 5 \text{ mm}^2$, centered on the rear face. Values of indices of refraction are chosen at 2.22 for the crystal and 1.7 for the photodetector (that is in fact the highest realistic value for the coupling material). With these conditions, detectable photons are always in total reflection on the lateral faces of the crystal, (moreover, some photons can never escape the crystal) thus one does not simulate any lateral wrapping. For the front and rear faces, in order to access the extreme characteristics of crystals, one investigates – refractive surfaces (with only Fresnel reflections), – perfectly reflecting surfaces, – and perfectly diffusive wrapping.

For the monitoring light, photons are generated outside the crystal, at the center of the front face, as if they were emitted by an optical fibre of negligible diameter and angular aperture 20° in air with a angular density approximated by a parabola. In a first step, absorbing rear and front faces are simulated to obtain the direct transmission, as above defined. Then, in a second step, simulations with reflections or diffusions on extremities give the total transmission.

For the scintillation light, photons are generated isotropically and uniformly over the surface of the crystal section at $z = 5, 25, 45\dots, 205, 225 \text{ mm}$. (z is counted from the front face, opposite to the photodetector.) In the same way, one first simulates absorbing rear and front faces to get the direct transmission, then reflection or diffusion on the front face are introduced to obtain the direct + back transmission, before to allow reflection or diffusion on both extremities to access the total transmission.

In a third step, as reported in section 3.3, the effective light yields are simulated for densities of light emission corresponding to typical electromagnetic shower energy profiles [10], using the same optical characteristics for the crystal.

Data are fitted with the above equations : 13, 13 + 14 and 17 for the scintillation light, 4 and 9 for the monitoring light, also by steps : C_{s_D} and b_{s_d} are extracted from the simulation with absorbing ends, then used as fixed to extract C_{s_B} and b_{s_b} from the simulation with reflecting or diffusing front face, then these fourth first values used to calculate k_s and b_s . The same step procedure is employed for C_{m_D} , b_{m_d} , k_m and b_m . This procedure is illustrated in figures 2 and 3.

In all the cases studied, the analytical model describes well the simulations. For the scintillation light, the variation of parameters with z are well described by an exponential for C_{s_D} and C_{s_B} , depending on the geometry. The other parameters have a small z variation, more or less linear. Figures 4 and 5 summarize these results for crystals with refractive and diffusive ends respectively. The value of the fitted parameters are reported in tables 1 for the monitoring light, 2 and 3 for the scintillating light.

Table 1: Values of the fitted parameters C_{m_D} , b_{m_d} , k_m and b_m for crystals with perfectly refractive diffusive and refractive ends and without chamfers.

		tapered crystal	parallelepipedic crystal
	C_{m_D}	0.03874(2)	0.03876(1)
	b_{m_d}	1.005(1)	1.005(1)
refractive ends	k_m	0.121(2)	0.133(2)
	b_m	0.84(14)	0.96(13)
diffusive ends	k_m	0.9770(1)	0.9770(1)
	b_m	1.097(1)	1.088(1)
reflective ends	k_m	0.9766(1)	0.9767(1)
	b_m	1.379(1)	1.021(1)

Table 2: Values of the fitted parameters C_{s_D} , b_{s_d} , C_{s_B} , b_{s_b} , k_s and b_s for a crystal with perfectly refractive ends and without chamfers. ($z_r = z/L$)

	tapered crystal	parallelepipedic crystal
C_{s_D}	0.007300(4) $\exp(0.394(1)(1 - z_r))$	0.007369(4) $\exp(-0.002(1)(1 - z_r))$
b_{s_d}	1.267(2) - 0.050(4) z_r	1.203(2) + 0.015(4) z_r
C_{s_B}	0.005891(7) $\exp(0.421(2)(1 - z_r))$	0.005470(6) $\exp(0.000(2)(1 - z_r))$
b_{s_b}	1.349(3) - 0.009(6) z_r	1.279(4) - 0.002(7) z_r
k_s	0.9728(1) - 0.0016(1) z_r	0.9728(1) + 0.0002(1) z_r
b_s	1.721(2) + 0.027(3) z_r	1.545(2) + 0.028(3) z_r

Table 3: Values of the fitted parameters C_{s_B} , b_{s_b} , k_s and b_s for a crystal with perfectly diffusive ends and without chamfers. C_{s_D} , b_{s_d} are shown in table 2. ($z_r = z/L$)

	tapered crystal	parallelepipedic crystal
C_{s_B}	0.007278(7) $\exp(0.397(2)(1 - z_r))$	0.007354(7) $\exp(0.000(2)(1 - z_r))$
b_{s_b}	1.280(3) - 0.006(5) z_r	1.210(3) + 0.003(5) z_r
k_s	0.9793(1) - 0.0005(1) z_r	0.9786(1) + 0.0000(1) z_r
b_s	1.288(2) - 0.023(2) z_r	1.197(1) + 0.000(2) z_r

Table 4: Values of the fitted parameters C_{s_B} , b_{s_b} , k_s and b_s for a crystal with perfectly reflective ends and without chamfers. C_{s_D} , b_{s_d} are shown in table 2. ($z_r = z/L$)

	tapered crystal	parallelepipedic crystal
C_{s_B}	0.007286(7) $\exp(0.396(2)(1 - z_r))$	0.007367(7) $\exp(-0.001(2)(1 - z_r))$
b_{s_b}	1.280(3) + 0.002(5) z_r	1.212(3) + 0.007(5) z_r
k_s	0.9790(1) - 0.0004(1) z_r	0.9784(1) + 0.0000(1) z_r
b_s	1.299(2) - 0.027(2) z_r	1.192(1) - 0.001(1) z_r

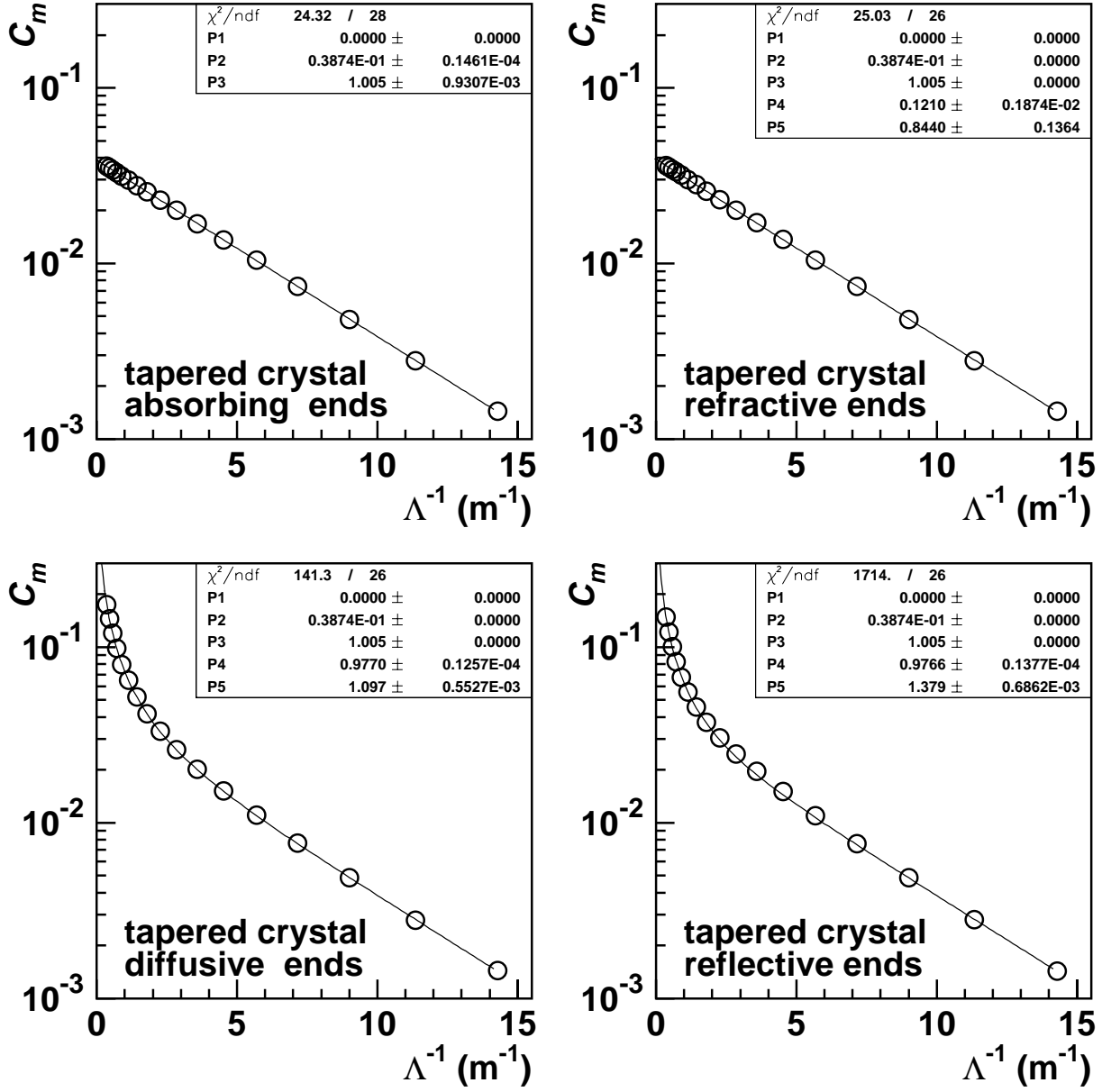


Figure 2: Variation of the monitoring light transmission C_m with the absorption coefficient Λ^{-1} : simulation of the light monitoring on a tapered, CMS shape, crystal without chamfers and respectively absorbing, refractive, reflective and diffusive ends, and fit by expressions 4 and 9 with $P1 = 0$, $P2 = C_{mD}$, $P3 = b_{m_d}$, $P4 = k_m$ and $P5 = b_m$.

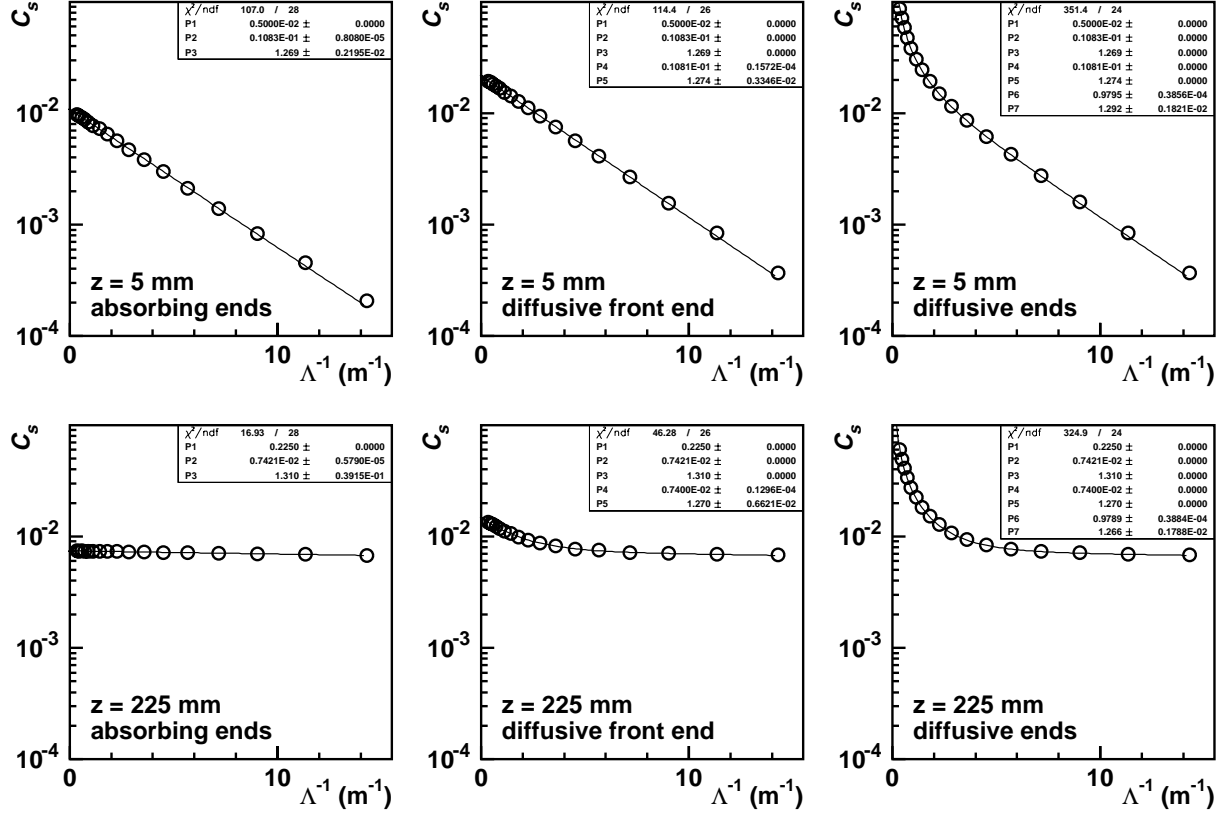


Figure 3: Variation of the scintillation light transmission C_s with the absorption coefficient Λ^{-1} : simulation of the scintillation emitted locally at a distance $z = 5$ and 225 mm from the front end, on a tapered, CMS shape, crystal without chamfers and diffusive ends, and fit by expressions 13, 14 and 17 with $P1 = z$, $P2 = C_{sD}$, $P3 = b_{s_d}$, $P4 = C_{sB}$, $P5 = b_{s_b}$, $P6 = k_s$ and $P7 = b_s$.

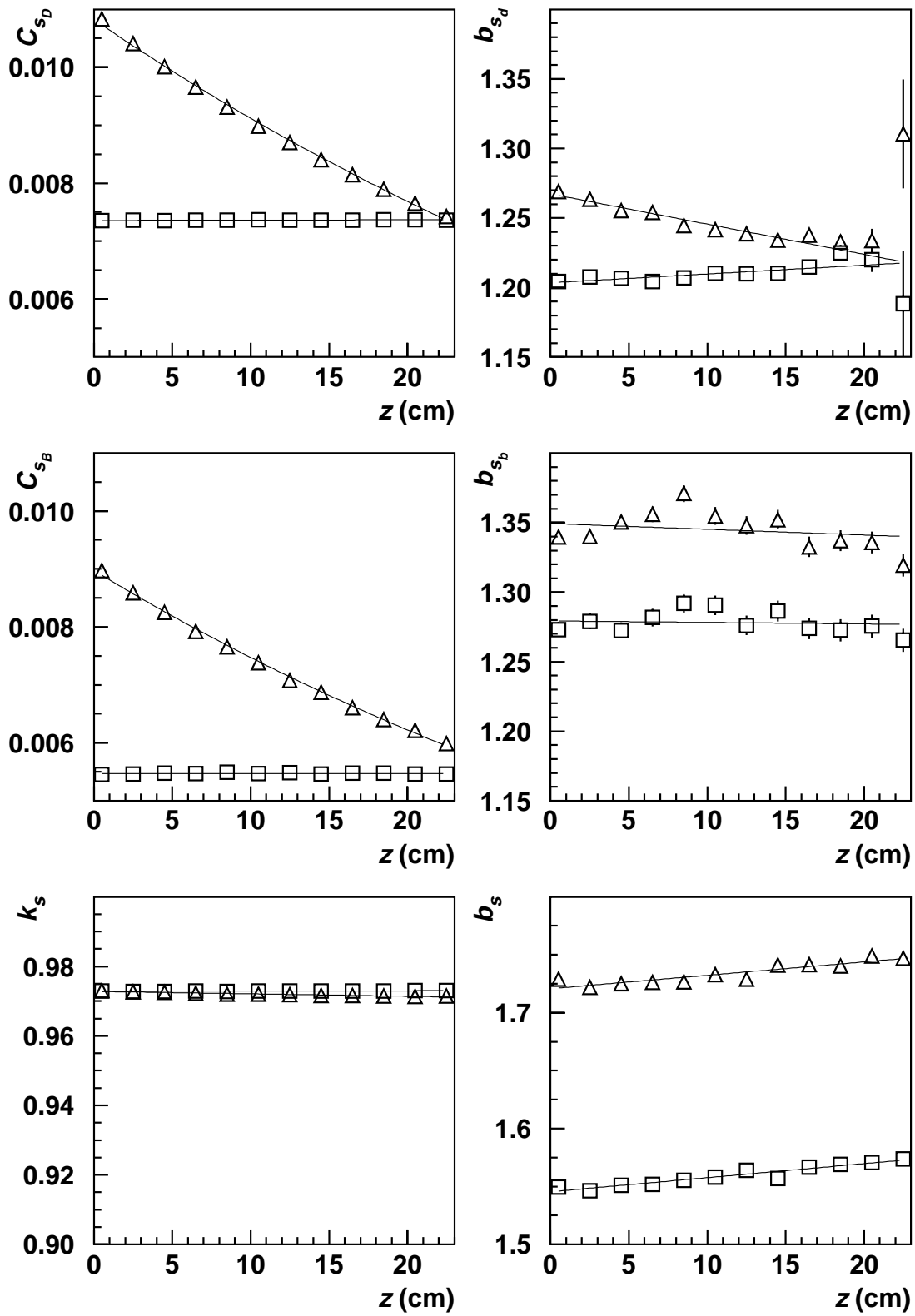


Figure 4: Variation of the parameters C_{sD} , b_{sD} , C_{sB} , b_{sB} , k_s and b_s with the distance of emission z (the photodetector being at $z = 23$ cm) in a crystal with refractive ends. Open triangles : tapered crystal without chamfer, open squares : parallelepipedic crystal without chamfer. Exponential fits for C_{sD} and C_{sB} , linear for the other parameters.

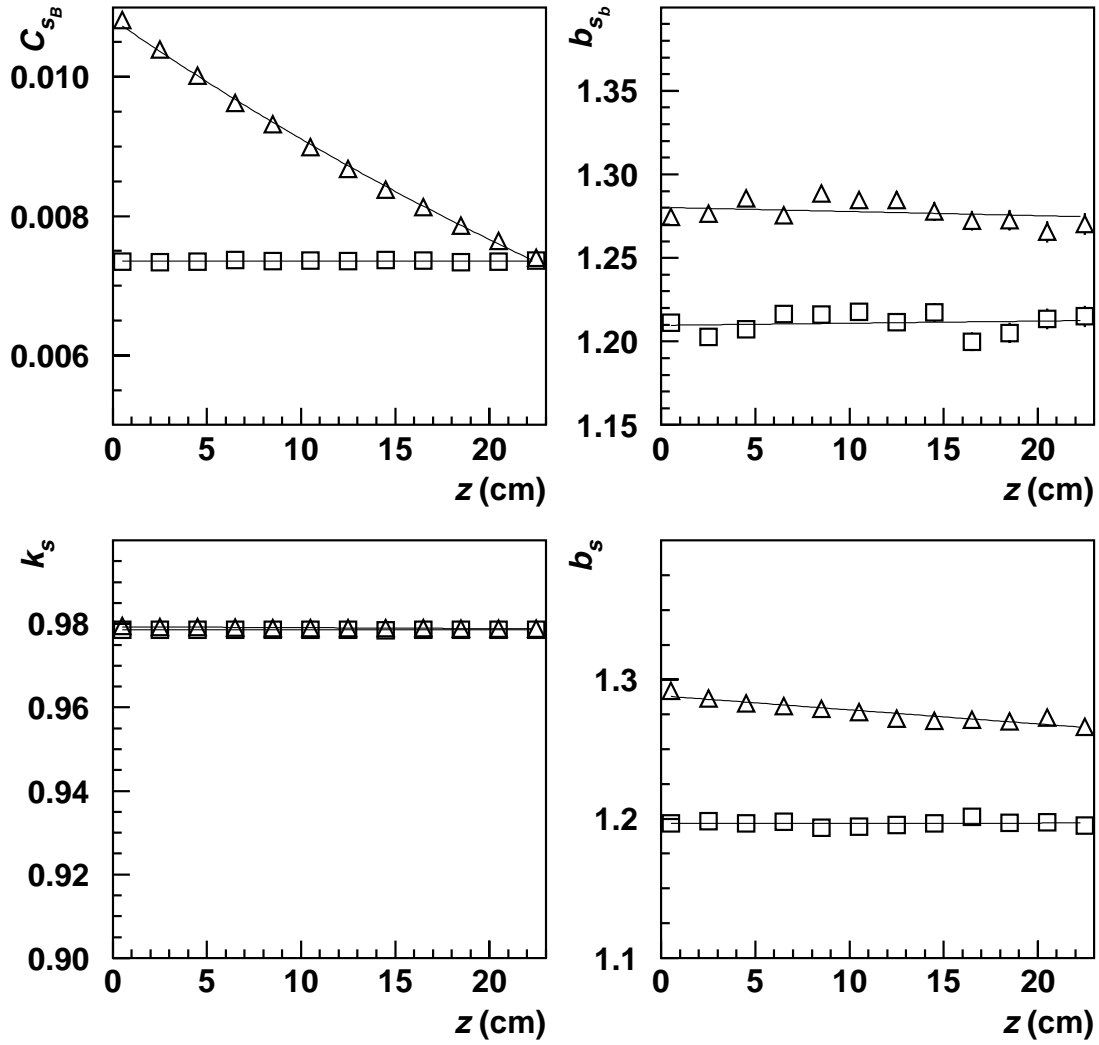


Figure 5: Variation of the parameters C_{sB} , b_{sB} , k_s and b_s with the distance of emission z (the photodetector being at $z = 23$ cm) in a crystal with diffusive ends. C_{sD} and b_{sD} are shown in figure 4. Open triangles : tapered crystal without chamfer, open squares : parallelepipedic crystal without chamfer. Exponential fits for C_{sB} , linear for the other parameters.

3.2 Discussion

As a general fact, data obtained with reflective and diffusive ends are qualitatively identical, and quantitatively very similar, indicating that this is mostly the efficiency of the reflection that is important, much more than it's specular or diffusive character. The solid angle in which the photons should strike the output crystal surface is very limited, despite the relatively high index value chosen in simulation for the coupling between photodetector and crystal. To not overload the discussion, the results on reflective ends will not be detailed hereafter.

Qualitatively speaking, the two different light transmissions behave as expected. Both have an exponential variation when absorbing ends are assumed, with a slope close to the distance between the emission point and the photodetector. Reflections on crystal ends introduce a curvature in the transmission variations in the low absorption region, obviously related to the detection of "multiple turn" light.

More quantitatively, the values of fitted parameters are well explained. For the monitoring light, no clear influence of the crystal geometry is seen, this light being always in total reflection on lateral faces. Due to reflections on lateral faces, C_{mD} is slightly over the ratio of photodetector area *versus* the rear end area weighted by partial reflections on front and rear ends, (which would give 0.03744 for rays normal to the ends). b_{m_d} is equal to what is expected on the ground of the angular density of the simulated fibre. k_m is in both cases closely given by the partial reflections on ends weighted by the surface ratio, (one obtains, for rays normal to the ends, effective reflection coefficients equal to 0.9779 for diffusive coating and 0.1407 for refractive ends. b_m is compatible with b_{m_d} for refractive ends, slightly increased for diffusive ends. Higher values were however expected, following the dispersion introduced by the diffuser and, as in the case of scintillation, the effective angular aperture of the photodetector.

For the scintillating light, the parameters derived for the parallelepipedic crystal are also closely related to what could be estimated. A first order calculation, not taking into account the variation of reflection with the incident angle would give in that geometry $C_{sD} = 0.078$ instead of 0.0737, and $b_{s_d} = 1.237$ instead of 1.203. In the case of diffusive ends, one has as expected $C_{sB} = C_{sD}$ and $b_{s_b} = b_{s_d}$. In the case of refractive ends, one should note that C_{sB} is not small, traducing the fact that an important fraction of the detectable scintillating light is however in total reflection on all faces of the crystal, including ends, unlike the monitoring light. One should have in fact $C_{sB} \simeq k_s C_{sD}$, which is not truly verified in our simulation. One explanation could be in the fact that contrary to the hypothesis of equations 16, the effective reflection coefficient for the first reflection of the direct light, ${}^o r_{s_{d1}}$, is much smaller than the others and should have been considered apart (as done with ${}^i r_{s_b}$ for the back light). This would lead to similar expressions, with more complex meaning for the fitted parameters.

The influence of crystal geometry is clearly seen in C_{sD} and C_{sB} and can be approximated by an absorption length Λ_{geom} , negative for C_{sD} and positive for C_{sB} . For the geometry simulated here, one obtain $\Lambda_{\text{geom}} = 2.53L$ for both direct and back lights, except for the crystal with refractive ends in which a slight difference is observed for the same reason as previously.

Small variations are observed in the effective length parameters b_{s_d} , b_{s_b} and b_s , due to the geometry. In general, effective lengths are slightly increased. No marked dependence with z is noted, except for the direct light coefficient b_{s_d} for which a small linear decrease is observed, directly

explained by the focusing effect. Thus one may rewrite equation 17 as :

$$C_s(t, \lambda, z) = \frac{C_{s_{D_0}} \exp\left(-\frac{b_{s_d}(L-z)}{\Lambda(t, \lambda) - \Lambda_{\text{geom}}}\right) + C_{s_{B_0}} \exp\left(-\frac{b_{s_b}(L+z)}{\Lambda(t, \lambda) + \Lambda_{\text{geom}}}\right)}{1 - k_s^2 \exp\left(-\frac{2b_s L}{\Lambda(t, \lambda)}\right)} \quad (18)$$

in which $C_{s_{D_0}}$, b_{s_d} , $C_{s_{B_0}}$, b_{s_b} , k_s , b_s and Λ_{geom} can be considered as independent of z . One has $b_{s_d} \simeq b_{s_b}$ and, when the ends are covered with diffusers or reflectors, $C_{s_{D_0}} \simeq C_{s_{B_0}}$.

3.3 Electromagnetic shower response

With these hypothesis, and assuming that the emission spectrum is constant over the crystal, integrations over z and λ in equation 2 can be separated, and one can define an effective light yield, ${}^{sh}C_s$ by :

$${}^{sh}C_s(E_0, t, \lambda) = \int_0^L N(E_0, z) C_s(t, z, \lambda) dz \quad (19)$$

With this simplification, the convolution in z resumes to a sum of two integrations over the crystal length of $N(E_0, z)$ times an exponential in z , which would be easy to calculate knowing a parameterisation of the shower energy profile.

However, at least for absorption length higher than the crystal length, a good approximation would be to consider that all behaves as if the light were emitted from the center of gravity of the shower, that is from a distance \bar{z}_{sh} . This can be derived easily in developing the exponentials at the first order in z/Λ

This is confirmed by the simulation of light yield for a electromagnetic shower, shown for example in figure 6 for a 50 GeV electron shower. This indicates that, for an electromagnetic shower, the variation of the scintillation response can be interpreted within the same scheme as previously, and that the light yield ${}^{sh}C_s$ can be described by the same equations 17 or 18 with global parameters. For example by :

$${}^{sh}C_s(t, \lambda) = \frac{{}^{sh}C_{s_D} \exp\left(-\frac{{}^{sh}b_{s_d}(L-\bar{z}_{\text{sh}})}{\Lambda(t, \lambda)}\right) + {}^{sh}C_{s_B} \exp\left(-\frac{{}^{sh}b_{s_b}(L+\bar{z}_{\text{sh}})}{\Lambda(t, \lambda)}\right)}{1 - {}^{sh}k_s^2 \exp\left(-\frac{2{}^{sh}b_s L}{\Lambda(t, \lambda)}\right)} \quad (20)$$

Assuming ${}^{sh}b_{s_d} = {}^{sh}b_{s_b}$ allows to determine a value of \bar{z}_{sh} from the fitted parameters. As shown in table 5, this z value is very close to the one predicted from the shower density ($\bar{z}_{\text{sh}} = 8.28$ mm for a 50 GeV electron shower). One finally obtains expressions in which parameters are very close to those that could be calculated with the formulæ of tables 2 and 3. This reinforce the validity of the model proposed here, whose main parameters are the absorption length and the effective reflection coefficients on the ends of the crystal.

One should also point out an important difference between the variation of scintillation and monitoring lights in crystals with or without diffusers/reflectors on their ends. In both cases, a significant part of the scintillating light could be back-reflected at the ends of the crystal, whereas only a very small part of the monitoring light is subject to the same treatment in naked crystals. This arises in figures 2 and 6 by the difference of curvature of the curves. In crystals

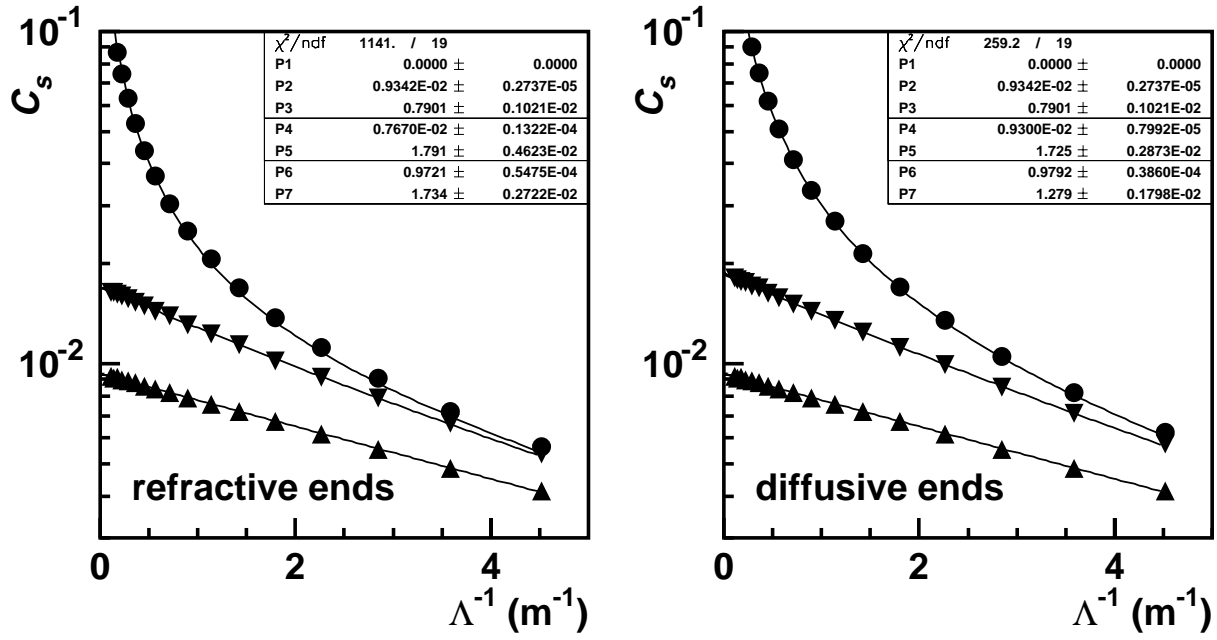


Figure 6: Variation of the light yield $^{sh}C_s$ with the absorption coefficient Λ^{-1} , simulated for an energy deposition profile of a 50 GeV electron. Same fits as in figure 3 except $P1 = 0$. Triangles : absorbing ends, reverse triangles : refractive or diffusive front end, absorbing rear end, circles : both ends refractive or diffusive.

Table 5: Values of the parameters $^{sh}C_{sD}$, $^{sh}b_{sd}$, $^{sh}C_{sB}$, $^{sh}b_{sb}$, $^{sh}k_s$, $^{sh}b_s$ and \bar{z}_{sh} for crystals with perfectly refractive, diffusive or reflective ends and without chamfers, as fitted from the simulation data and calculated from formulæ and data of tables 2 and 3.

	refractive ends		diffusive ends		reflective ends	
	fitted parameters	calculated parameters	fitted parameters	calculated parameters	fitted parameters	calculated parameters
$^{sh}C_{sD}$	0.009342(3)	0.009290(13)	0.009342(3)	0.009348(11)	0.009342(3)	0.009352(11)
$^{sh}C_{sB}$	0.007670(13)	0.007622(19)	0.009300(8)	0.009339(16)	0.009279(11)	0.009341(17)
$^{sh}b_{sd}$	1.291(2)	1.237(2)	1.258(2)	1.238(2)	1.256(2)	1.238(2)
$^{sh}b_{sb}$	1.291(2)	1.346(4)	1.258(2)	1.278(3)	1.256(2)	1.281(3)
$^{sh}k_s$	0.9721(1)	0.9722(1)	0.9792(1)	0.9791(1)	0.9790(1)	0.9789(1)
$^{sh}b_s$	1.734(3)	1.731(2)	1.279(2)	1.280(1)	1.287(2)	1.289(3)
\bar{z}_{sh}	8.92(3) cm	8.28 cm	8.55(2) cm	8.28 cm	8.53(2) cm	8.28 cm

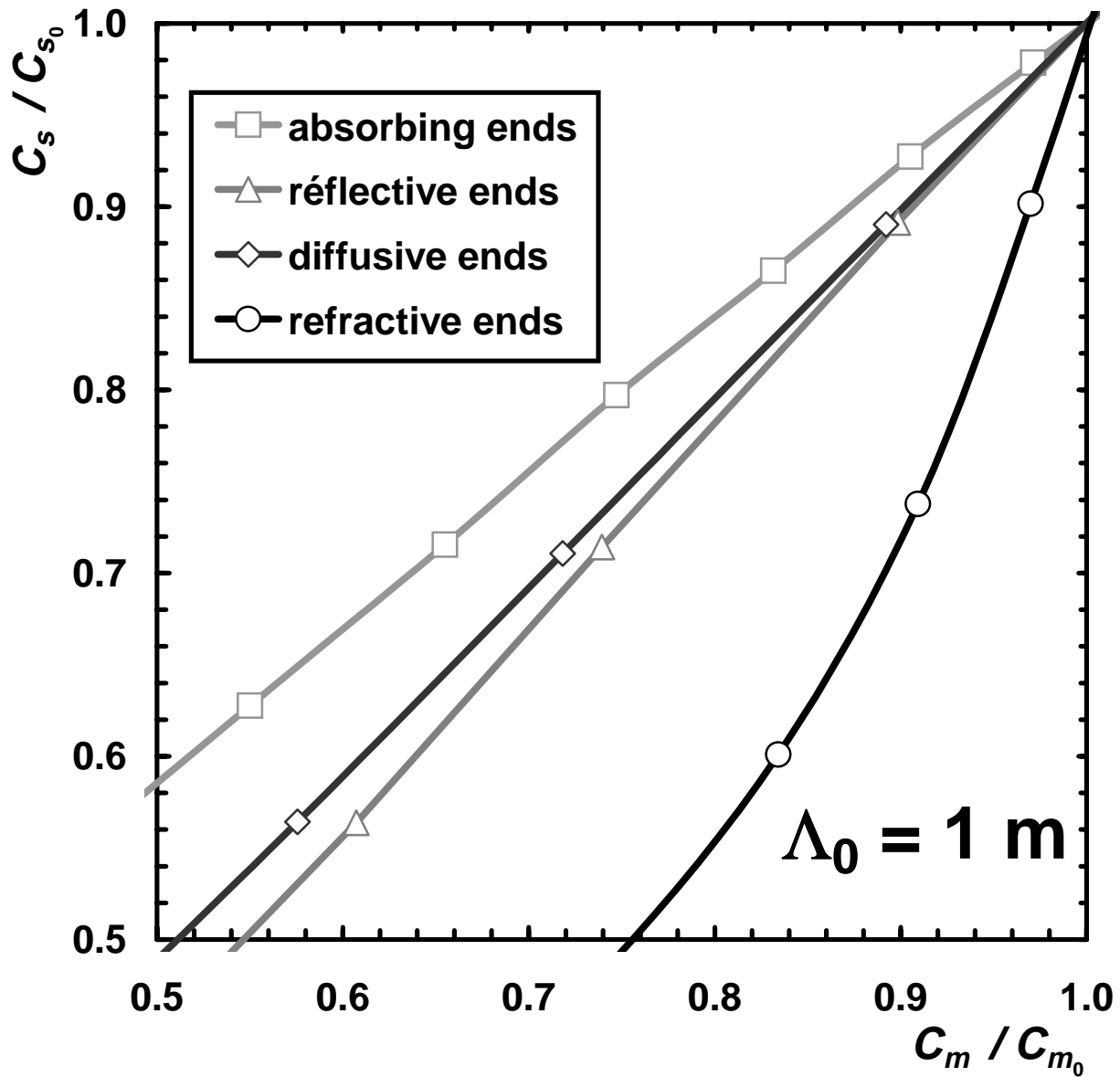


Figure 7: Correlation between scintillation light and monitoring light variations, for a 50 GeV electron shower in a tapered crystal without chamfers, assuming an initial absorption length $\Lambda_0 = 1 \text{ m}$ and a same absorption variation for scintillation and monitoring *i.e.* a same effective wavelength.

with diffusive or reflective ends, as obviously also in crystals with absorbing ends, the variations of scintillating and monitoring lights are almost proportional, – apart, at the first order, the ratio $^{sh}b_s(1 - \bar{z}_{sh})/b_m$ and an eventual difference in wavelengths inducing different absorptions –, whereas, with refractive ends, the scintillating light decreases in proportion much more rapidly than the monitoring light at low absorption.

This is illustrated in figure 7. This also explain, at least qualitatively, the correlation observed in ageing beam tests, in which a factor two between calibration and monitoring variations ($(\Delta S_s(t)/S_s(t))/(\Delta S_m(t)/S_m(t)) \approx 2$) is commonly observed [11], as a result of the poor reflectivity of the coating of crystal ends. Figure 8 indicates that the slope of the correlation between scintillation and monitoring depends greatly on the optical quality of the crystal itself, but also on these of the coating of its extremities. In case of refractive coating, (*i.e.* if the coating absorbs the light), this slope can varies strongly with the initial absorption length, especially if this parameter is longer than a few crystal lengths. More detailed simulations and measurements have to be done to precise this point, crucial for the monitoring efficiency. However, this simulation strongly suggests to increase the reflectivity of the coating of crystal ends in the final set-up, to approach the ideal factor $(\Delta S_s(t)/S_s(t))/(\Delta S_m(t)/S_m(t)) = 1$.

4 Conclusion

The model proposed here is based on a few number of effective parameters : absorption length, mean path lengths (through b_m and b_s), reflection and transmission coefficients. One of its advantages is to disconnect effect of absorption from other optical parameters. In low absorption crystals, such as those which will be used in the CMS calorimeter, it shows that most of the light yield variation is due to the “multiple turn” light, – which justify the approximation of an homogeneous absorption –, and points out the great importance of the treatments of crystal extremities in the correlation between scintillation and monitoring variations. One has interest to use low absorption reflectors or diffusers, not only for the absolute light yield, but also to be close to the optimal scintillation/monitoring correlation, when one deal with low absorption crystals.

At that stage, the model describes well the simulations performed on crystals with polished faces. On crystals with one lateral face polished, – as foreseen in the CMS calorimeter –, or more generally on “uniformized” crystals, one can nevertheless presume that the same argumentation can be employed, due to the fact that this model relies on mean, effective, transmission and reflections parameters. One other strong argument is also the *de facto* small angular aperture of the photodetection, even lower in reality with coupling refractive index rather close to 1.5. This should be verified in further simulations.

Acknowledgements

This work take place in the CMS ECAL monitoring development project.

We acknowledge numerous and fruitful discussions with J.-P. Pansart, J. Rander and P. Rebourgeard. We also thank warmly A. Givernaud, who provided the energy deposition profile data.

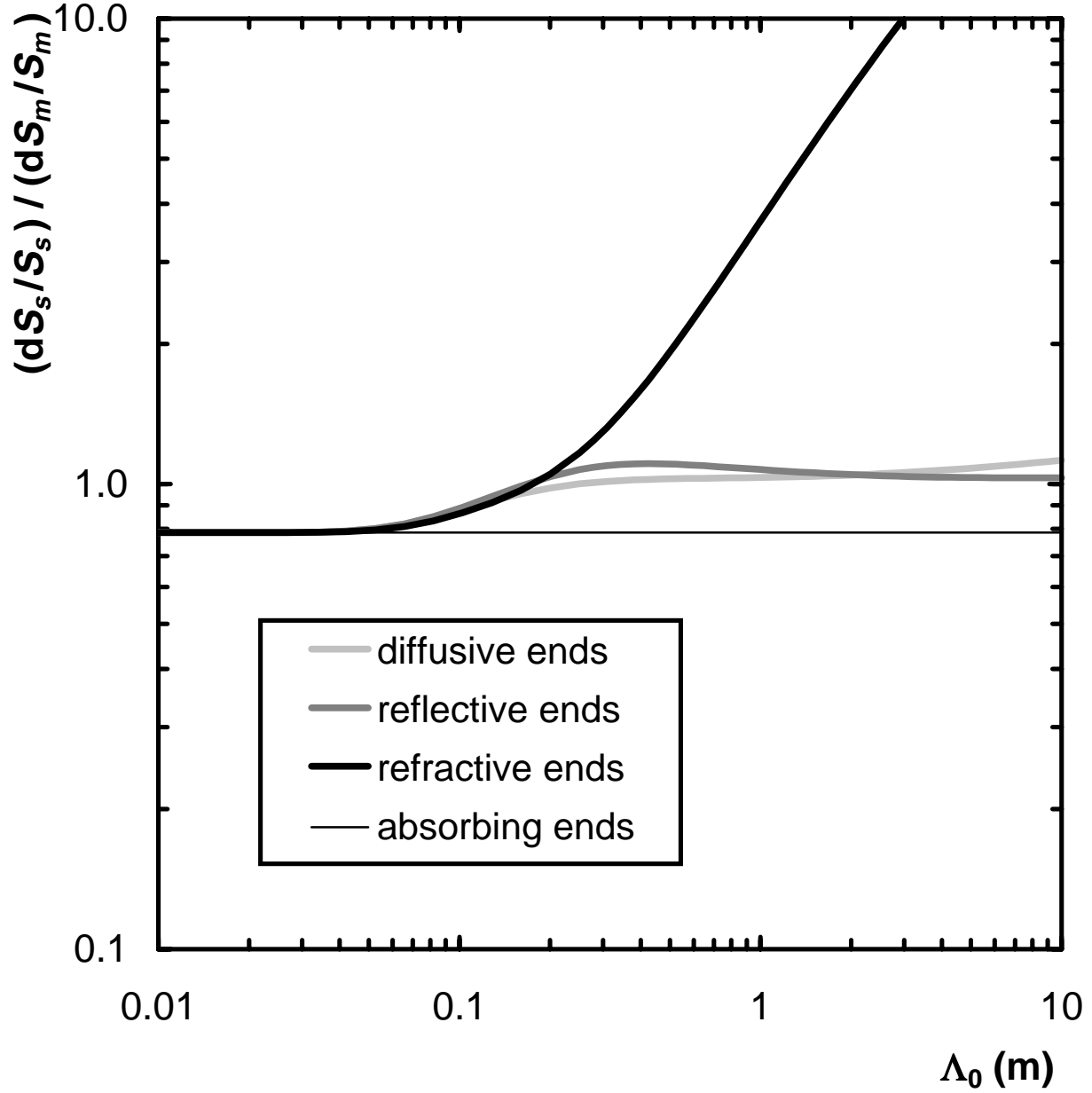


Figure 8: Variation of the slope $(d^{sh}S_s(\Lambda)/^{sh}S_s(\Lambda))/(dS_m(\Lambda)/S_m(\Lambda))|_{\Lambda=\Lambda_0}$ of the correlation between scintillation light and monitoring light variations, for a 50 GeV electron shower in a tapered crystal without chamfers, assuming a same absorption variation for scintillation and monitoring, *i.e.* a same effective wavelength, calculated from equations 9 and 20.

References

- [1] CMS collaboration, “*The Compact Muon Solenoid – Technical Proposal*”, CERN/LHCC 94–38, LHCC/P1 (1994).
- [2] CMS collaboration, “*The Electromagnetic Calorimeter Project – Technical Design Report*”, CERN/LHCC 97–33, CMS TDR 4 (1997).
- [3] P. Verrecchia, Nuclear Physics B (Proc. Suppl.), 61B (1998) 71–76.
- [4] P. Bonamy et al., “*The ECAL calibration : Use of the light monitoring system. Version 2.0*”, CMS NOTE–1998/013 (1998).
- [5] N. Annenkov et al., “*Systematic study of the $PbWO_4$ crystal short term instability under irradiation*”, Radiation Measurements, 29 (1998) 27–38.
- [6] M. Géléoc, *Étude du système de suivi optique des cristaux scintillants du calorimètre électromagnétique de l’expérience CMS*, Thesis, Université Paris–VII, 1998.
- [7] R. Chipaux et al., “*Results of a laboratory test of the CMS electromagnetic calorimeter monitoring correction*”, in preparation, to be submitted to Nucl. Instrum. and Meth.
- [8] E. Auffray et al., “*Scintillation characteristics and radiation hardness of PWO scintillators to be used in the CMS electromagnetic calorimeter at CERN*”, in : Proc. Int. Conf. on Inorganic Scintillators and their Applications, SCINT 95, P. Dorenbos and C.W.E. van Eick eds., Delft University Press, 1996, p 282–285.
- [9] R.Y. Zhu et al., in : Proc. 6th Int. Conf. on Calorimetry in High Energy Physics, Frascati 1996, A. Antonelli et al. eds., Frascati Physics Series, 1996, p 577.
- [10] A. Givernaud, personal communication.
- [11] P. Verrecchia, personal communication.